

## Scalp EEG functional connection and brain network in infants with West syndrome<sup>☆</sup>



Runze Zheng <sup>a,b</sup>, Yuanmeng Feng <sup>a,b</sup>, Tianlei Wang <sup>a,b</sup>, Jiuwen Cao <sup>a,b,c,\*</sup>, Duанпо Wu <sup>a,d</sup>, Tiejia Jiang <sup>e</sup>, Feng Gao <sup>e</sup>

<sup>a</sup> Machine Learning and I-health International Cooperation Base of Zhejiang Province, Hangzhou Dianzi University, 310018, China

<sup>b</sup> Artificial Intelligence Institute, Hangzhou Dianzi University, Zhejiang, 310018, China

<sup>c</sup> Research Center for Intelligent Sensing, Zhejiang Lab, Hangzhou, Zhejiang, 311100, China

<sup>d</sup> School of Communication Engineering, Hangzhou Dianzi University, Hangzhou 310018, China

<sup>e</sup> Department of Neurology, the Children's Hospital, Zhejiang University School of Medicine, National Clinical Research Center for Child Health, Hangzhou, 310003, China

### ARTICLE INFO

#### Article history:

Received 17 January 2022

Received in revised form 21 May 2022

Accepted 31 May 2022

Available online 7 June 2022

#### Keywords:

West epilepsy syndrome

Scalp EEG

Functional connection

Brain network

Network topology

### ABSTRACT

The common age-dependent West syndrome can be diagnosed accurately by electroencephalogram (EEG), but its pathogenesis and evolution remain unclear. Existing research mainly aims at the study of West seizure markers in time/frequency domain, while less literature uses a graph-theoretic approach to analyze changes among different brain regions. In this paper, the scalp EEG based functional connectivity (including Correlation, Coherence, Time Frequency Cross Mutual Information, Phase-Locking Value, Phase Lag Index, Weighted Phase Lag Index) and network topology parameters (including Clustering coefficient, Feature path length, Global efficiency, and Local efficiency) are comprehensively studied for the prognostic analysis of the West episode cycle. The scalp EEGs of 15 children with clinically diagnosed string spasticity seizures are used for prospective study, where the signal is divided into pre-seizure, seizure, and post-seizure states in 5 typical brain wave rhythm frequency bands ( $\delta$  (1–4 Hz),  $\theta$  (4–8 Hz),  $\alpha$  (8–13 Hz),  $\beta$  (13–30 Hz), and  $\gamma$  (30–80 Hz)) for functional connectivity analysis. The study shows that recurrent West seizures weaken connections between brain regions responsible for cognition and intelligence, while brain regions responsible for information synergy and visual reception have greater variability in connectivity during seizures. It is observed that the changes in  $\beta$  and  $\gamma$  frequency bands of the multiband brain network connectivity patterns calculated by Corr and WPLI can be preliminarily used as judgment of seizure cycle changes in West syndrome.

© 2022 Elsevier Ltd. All rights reserved.

## 1. Introduction

West syndrome, known as Infantile spasms, is the most common age-dependent epileptic encephalopathy. West syndrome usually occurs in infancy and early childhood (Cui, Cao et al.,

2022; Feng et al., 2022; Pavone et al., 2020). The typical clinical manifestation of West is a sudden contractions of the trunk and limbs, followed by a brief tonic contractions. The recurrent epilepsy can cause children to suffer from various neurological diseases, such as mental movement disorders, developmental delay or decline (Pavone, Striano, Falsaperla, Pavone, & Ruggieri, 2014), and may evolve into more serious epilepsy diseases, such as Lennox–Gastaut syndrome. The cause of West is complicated, the pathogenesis and evolution process are not clear so far, and accurate and effective treatment cannot be performed clinically (Janicot, Shao, & Stafstrom, 2020). Only few children have normal cognitive and motor development, but severe and frequent seizures will permanently damage the cognitive, learning, and language functional areas of the brain in most patients (Capone, Goyal, Ares, & Lannigan, 2006). Therefore, exploring the effects of infantile spastic seizures on functional brain areas is critical, that can promote clinical diagnosis and research on pathogenesis.

<sup>☆</sup> This work was supported by the National Key Research and Development Program of China (2021YFE0100100, 2021YFE0205400), the National Natural Science Foundation of China (U1909209, 62003119), the Key Research and Development Program of Zhejiang Province (2020C03038), the Natural Science Key Foundation of Zhejiang Province (LZ22F030002), the Open Research Projects of Zhejiang Lab (2021MC0AB04), and the Zhejiang Provincial Natural Science Foundation (LBY21H090002, LBY21H090001).

\* Corresponding author at: Machine Learning and I-health International Cooperation Base of Zhejiang Province, Hangzhou Dianzi University, 310018, China.

E-mail addresses: [runzewuyu@hdu.edu.cn](mailto:runzewuyu@hdu.edu.cn) (R. Zheng), [jsnt\\_fym@126.com](mailto:jsnt_fym@126.com) (Y. Feng), [tianleiwang@hdu.edu.cn](mailto:tianleiwang@hdu.edu.cn) (T. Wang), [jwcao@hdu.edu.cn](mailto:jwcao@hdu.edu.cn) (J. Cao), [wuduanspo@hdu.edu.cn](mailto:wuduanspo@hdu.edu.cn) (D. Wu), [jiangyouze@zju.edu.cn](mailto:jiangyouze@zju.edu.cn) (T. Jiang), [epilepsy@zju.edu.cn](mailto:epilepsy@zju.edu.cn) (F. Gao).

**Table 1**

EEG and clinical features of participants included in the analysis (M: month, D: days, M: Male, F: Female, h: hour, min: minutes, s: seconds), the frame length is 2 s.

ID	Age	Gender	Number of episodes	Number of samples	Recording time
1	7M	M	1	180	2 h 22 min 26 s
2	12M	F	1	55	2 h 38 min 30 s
3	13M	M	1	201	2 h 13 min 05 s
4	21M	F	2	74	1 h 57 min 14 s
5	12M	F	1	89	1 h 58 min 13 s
6	6M16D	M	2	436	14 h 41 min 32 s
7	13M	F	1	168	2 h 03 min 31 s
8	11M17D	M	1	71	1 h 46 min 50 s
9	7M8	M	2	330	2 h 36 min 46 s
10	11M16D	F	1	155	1 h 29 min 13 s
11	6M25D	F	1	97	2 h 29 min 53 s
12	18M	F	1	122	2 h 10 min 13 s
13	13M	M	1	42	1 h 57 min 34 s
14	11M12D	F	1	70	1 h 34 min 51 s
15	6M17D	F	3	347	2 h 01 min 53 s

Scalp Electroencephalography (EEG) has been widely used in West syndrome analysis for its high practicability and low cost. Chu et al. (2021) proposed multi-scale entropy as an objective biomarker of abnormal EEG in infantile spasms, and analyzed whether it is related to treatment response and seizure outcome before and after treatment. Bernardo, Nariai, Hussain, Sankar, and Wu (2020) proved that the phase coupling of high-frequency oscillation and slow-wave activity can be used as a potential marker for West prognostic treatment. Similarly, McCrimmon et al. (2021) used the scalp high-frequency oscillations to accurately identify West subjects from healthy. Although, the characteristics of EEGs are very useful for clinical diagnosis of West as biomarkers (Cao, Zhu, Hu, & Kummert, 2020; Hu, Cao, Lai, Liu et al., 2020; Hussein, Lee, Ward, & McKeown, 2021; Raghu, Sriraam, Temel, Rao, & Kubben, 2020; Wen et al., 2021; Xu et al., 2021), these objective patterns are usually not conducive to understand the underlying neural mechanism of West.

Graph theory has been recently applied in the brain imaging, electrophysiology and epilepsy analysis for its ability in quantifying the characteristics of complex system topologies (Bernhardt, Bonilha, & Gross, 2015; Stacey et al., 2020). Guo et al. (2021) achieved the detection of high frequency oscillations for stereoelectroencephalography (SEEG) in epilepsy using the hypergraph learning. Li, Sohrabpour, Jiang, and He (2021) proposed a novel approach to model the temporal-spatial-spectral dynamics of cross-frequency coupling (CFC) networks, where graph measures were used to characterize the high-frequency and low-frequency hubs in treatment outcome of epilepsy. Lin et al. (2021) used the spatial pattern of network (SPN) features of resting-state scalp EEGs from the functional and effective EEG networks to achieve medically controlled epilepsy classification. Rosch, Baldeweg, Moeller, and Baier (2018) designed a dynamic tracking model, revealing the correlation between early epileptic encephalopathy and the dynamic characteristics of the brain network. In general, the quantitative analysis of brain network can help to understand the neurobiological mechanism for clinical diagnosis.

For West syndrome, only a few research on graph networks have been reported in the past. For instance, Hu, Mower, Shrey and Lopour (2020) used linear cross-correlation coefficients to construct functional connection network to analyze the influence of interictal epileptiform discharges in West syndrome. It is found that the connection strength of brain network in interictal epileptiform discharges is enhanced. Shrey et al. (2018) studied the changes in brain network of West syndrome, and concluded that changes in network connectivity and stability

are related to the treatment response. Meanwhile, pre-treatment connectivity is very beneficial for the prediction of short-term treatment response. But the brain network functional connection of existing studies is generally evaluated using simple linear correlation coefficient. Moreover, existing studies mainly analyzed the prognostic control of West with a small number of patients. The changes in brain network connectivity patterns during the West seizure cycle are not well studied.

In this paper, we aim to analyze the scalp EEG functional connectivity and network topology in the prognosis of West seizure cycle, and also to explore the pathogenesis of West syndrome. The analysis is conducted on scalp EEGs of 19 channels, where the electrode leads are assigned as network nodes and the features on 5 sub-bands of EEGs ( $\delta$ ,  $\theta$ ,  $\alpha$ ,  $\beta$ ,  $\gamma$ ) are extracted for analysis (Cao, Chen et al., 2021; Cao, Hu, Yaomin, Wang & Lei, 2021; Cui, Hu et al., 2022; Hu, Cao, Lai, Wang et al., 2020; Wang, Cao, Hu, Jiang, & Gao, 2021). The connection matrices and weighted networks based on correlation, coherence, Time Frequency Cross Mutual Information (TFCMI), Phase-Locking Value (PLV), Phase Lag Index (PLI), Weighted Phase Lag Index (WPLI) are constructed from the constituent components of EEGs (amplitude, frequency, phase angle). A two-tailed t-test is adopted to detect the intensity of brain area connectivity patterns in the West seizure cycle. To assess the efficiency of brain networks in processing global and local information during West seizure cycles, 4 network topological parameters, Clustering coefficient (C), Global efficiency (Ge), Local efficiency (Le), Feature path length (Pl), are derived. The stage differences in local and global efficiency of brain network in 5 sub-bands during the seizure cycle are observed. The study on 15 West syndrome children shows that:

- During the seizure cycle, there is asymmetry in connectivity between the left and right brain regions.
- Significant changes in the strength of connectivity between parietal and occipital regions, frontopolar and temporal lobe regions can be observed.
- Changes in brain area connectivity patterns and network parameters in  $\delta$  band could be employed to determine West seizure cessation prognosis.
- Through correlation and WPLI obtained from multiband brain network connections, changes in the  $\beta$  and  $\gamma$  frequency bands could be effectively applied for West seizure prediction.

Fig. 1 shows the overall framework for functional connection and brain network analysis on West syndrome in this paper. There mainly include 4 parts for the analysis: (A) Data collection for West syndrome subjects, (B) EEG preprocessing and artifact removal, (C) Representative correlation feature extraction, and (D) Functional connectivity analysis and result evaluation.

## 2. Data collection

### 2.1. Subject identification

The purpose of this study is to establish different brain network patterns to analyze the changes in brain areas before and after a series of spasms. The data of West patients are selected from standard pediatric clinical EEGs, labeled by clinical neurophysiologists with expertise in pediatric EEG. Table 1 details the participant information. The average age of the patients is 11 months, the male to female ratio was 2:3, and all have at least one spastic seizure. The main basis for patient subject selection is: (1) the clinical diagnosis of epilepsy is West syndrome, (2) the seizure pattern is a series of spastic seizures without prognostic control, (3) abnormal EEG data removal caused by loose lead connection, amplifier disconnection, etc. For analysis, the EEGs

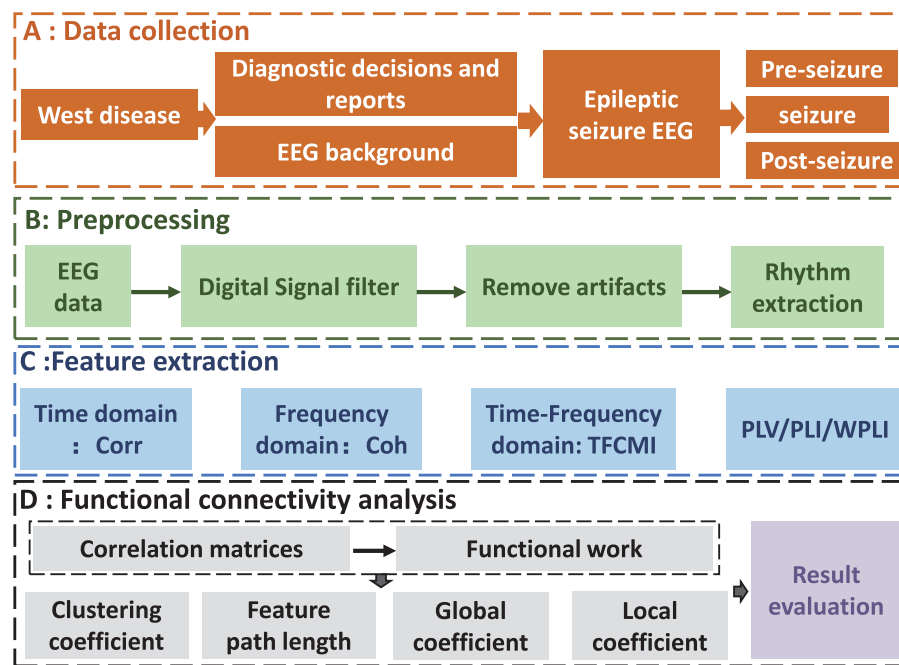


Fig. 1. Scalp EEG based functional connection and brain network analysis framework for West syndrome.

of 10 min before and after the seizure onset of the patients are extracted as the control group with respect to seizure EEGs. There are 3 different states: pre-seizure, seizure, and post-seizure, where the continuous EEG segments are used for analysis. The EEG of the patient is displayed in the form of reference leads. It can be clearly seen from Fig. 2 that the EEG pattern of West patient is highly arrhythmic in the pre-seizure and post-seizure stages. The 3 states are mixed with more high-frequency activity components.

All EEG recordings were performed with the informed consent of the legal guardian of the patient. To avoid revealing patients' privacy, we remove patients' names from the database. Only the EEGs, age, gender as well as the seizure onset times are remained for analysis. This study has been reviewed and approved by the Children's Hospital, Zhejiang University School of Medicine and Hangzhou Dianzi University.

## 2.2. EEG recordings

The patient's EEG data was collected in a quiet ward environment accompanied by parents, and all the data were recorded from the Children's Hospital, Zhejiang University School of Medicine. Using the NicoletOne EEG system (Nicolet V32, USA), EEG signal activity up to 1000 Hz is recorded for approximately 2 or 16 h with the Fpz electrode as the reference. Surface electrical signals of brain regions are not collected in A1 and A2 channels. The single-channel connection mode is used in this study. According to experimental analysis requirements, EEGs of 19 channels (Fp1, Fp2, F3, F4, F7, F8, C3, C4, T3, T4, P3, P4, T5, T6, O1, O2, Fz, Cz and Pz) are used, where F, T, P, O, z stand for frontal lobe, temporal lobe, parietal lobe, occipital lobe, midline, the odd and even numbers represent left and right scalp regions, respectively.

During seizure onset, unconscious subject movements, such as frowning and gnashing of teeth, will affect EEGs. Since these EEG artifacts can characterize the behavioral activities of during seizures, aiming to have a precise analysis in functional partition connectivity changes before and after seizure onset, the unconscious subject movements induced EEG artifacts are remained in

the analysis. The experiment is carried out on MATLAB R2019a platform, including data segmentation, bandpass (1–80 Hz) and 50-Hz trap filtering, etc. The 4th order IIR mid-pass filter is performed on EEG to extract the 5 brain rhythms. A sliding window with a time length of 2 s is employed to segment the data without overlap. The down-sampling method is used for sample balancing of 3 periods. For each subject, the same number of samples to seizure is randomly selected from pre-seizure and post-seizure periods, respectively. Particularly, 2437 samples are taken in each state for analysis. The details are shown in Table 1.

## 3. Methodology

To overcome the inherent limitations of EEGs, such as low spatial resolution, the time, space, and frequency domain characteristics are fully exploited to construct the functional network based on 5 typical brain rhythms for West seizure cycle analysis. Different brain rhythm information will be first extracted. The connections used to construct the EEG functional network are partially based on the signal phase angles from Hilbert transform.

### 3.1. EEG pre-processing

#### 3.1.1. Brain rhythm signal extraction

Different areas of the human brain coordinate information communicated from different central systems to provide the basis for vital functions (such as learning, memory, cognition, and emotion) (Miltner, Braun, Arnold, Witte, & Taub, 1999). It is demonstrated that the generated different rhythms of brain waves are closely related to these important functions. Medically, brain waves are usually divided into 5 key sub-bands,  $\delta$  (1–4 Hz),  $\theta$  (4–8 Hz),  $\alpha$  (8–13 Hz),  $\beta$  (13–30 Hz), and  $\gamma$  (30–80 Hz). Particularly,  $\delta$  waves are caused by high amplitude neural oscillations and are the principal waveform of brain waves in infants and children. It is shown that  $\delta$  waves are associated with epileptiform discharge activity in the brain (Clarke, Barry, McCarthy, & Selikowitz, 2001).  $\theta$  waves are associated with various sleep and waking states, and

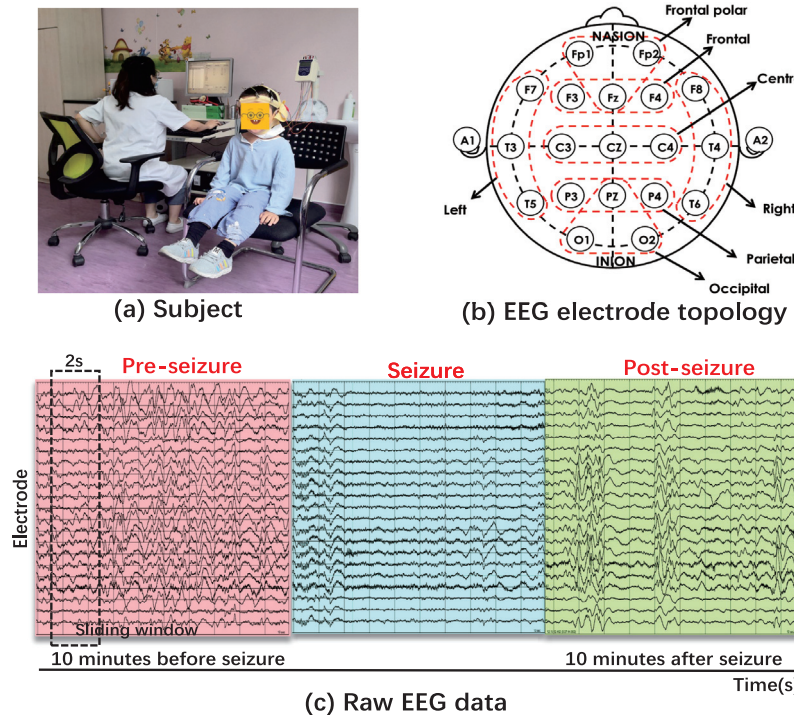


**Fig. 2.** EEGs of West syndrome in Pre-seizure, Seizure, and Post-seizure.

West seizures are more common after waking and before going to sleep.  $\theta$  wave dynamics features have been validated as the biomarker of epilepsy for patients with brain injury (Milikovsky et al., 2017).  $\alpha$  waves are generated through cortico-thalamic interactions and are associated with a large number of cognitive operations, particularly attention and memory (Abela et al., 2019). It is altered in neurological disorders commensurate with clinical severity. Hence, it is widely applied to monitor neurological dysfunction. Also, the phenomenon of  $\alpha$  waves slowing and anteriorization have been proven to be a general indicator of seizure tendency. On the motor cortex,  $\beta$  waves are relevant to muscle contractions that occur during isotonic movements and are inhibited before and during motor changes (Baker, 2007).  $\gamma$  waves are associated with large-scale brain network activity and cognitive phenomena, which are most prominent during alert, focused wakefulness (Hughes, 2008). It has been demonstrated that cognitive dysfunction in patients with seizures is strongly associated with  $\gamma$  waves activity.

### 3.1.2. Hilbert transform

Brain network analysis through the brain rhythms cannot well exclude the effect of wave amplitude and phase components of EEG. To solve this problem, the Hilbert transform is applied to EEG decomposition, instantaneous phase calculation, and brain network connection indicators construction based on phase synchronization (Oppenheim, 1999). The Hilbert transform is

$$z(t) = s(t) + j\hat{s}(t) = m(t) \cdot e^{j\theta(t)} \quad (1)$$

with  $m(t) = \sqrt{s^2(t) + \hat{s}^2(t)}$ ;  $\theta(t) = \arctan\left(\frac{\hat{s}(t)}{s(t)}\right)$ ,  $\hat{s}(t) = \frac{1}{\pi}$  p. v.  $\int_{-\infty}^{\infty} \frac{s(\tau)}{t-\tau} d\tau$ , where  $s(t)$  is brain rhythm signal,  $m(t)$  indicates the instantaneous amplitude,  $\theta(t)$  shows the instantaneous phase, p.v. represents the Corsi criterion value. It is clear that Hilbert transform extends the real signal  $s(t)$  to complex plane such that it satisfies the Corsi–Riemann equation. With (1), the phase angle of EEG signal at moment  $t$  can be calculated. For EEGs of two

channels  $x(t)$  and  $y(t)$ , their phase difference can be expressed as

$$\Delta\varphi_{xy}(t) = \theta_x(t) - \theta_y(t). \quad (2)$$

The two signals have a synchronization relationship if the phase difference is a constant. To evaluate signal synchronization based on phase difference, PLV, PLI, WPLI, etc., are widely used in biomedical signal processing.

### 3.2. Functional connectivity analysis

Complex brain functions often rely on functional and structural connectivity of the spatially separated brain regions. Epileptic disorders are caused by localized or mostly neuronal involvement in hyper-synchronous activity in these areas. When the degree of synchronization is higher, the shorter the duration of the waveform, the more neurons are involved in synchronization and the higher the EEG wave amplitude, resulting in the issuing of spikes or sharp waves. As the brain discharges become more, the normal brain activity will be affected (e.g. cognition, behavior, attention, etc.). Once the phenomenon is ended, the brain returns to normal. The spatial distributions are thus important indicators for EEG analysis. Subjects with epilepsy generally have diverse EEG feature distributions (e.g., generalization, diffuse, unilateral, localization). To analyze the spatial distribution of EEG in the three different states, we mapped the brain topography of each state separately using the average sample of all EEGs in Fig. 3. As the sample length is 2 s and the sampling frequency is 1000 Hz, for each millisecond, there has a brain topographic map for all three states. In the figure, we compared the brain topographic maps extracted from the averaged sample at 1 ms, 600 ms and 1200 ms, respectively. As observed, the amplitude of the anterior and posterior scalp regions varied considerably in the  $\delta$  and  $\theta$  frequency bands, whereas there has no obvious consistent changing patterns in the  $\alpha$ ,  $\beta$  and  $\gamma$  bands.

To quantify the functional brain network of West syndrome, EEG connection evaluation metrics calculated from the time

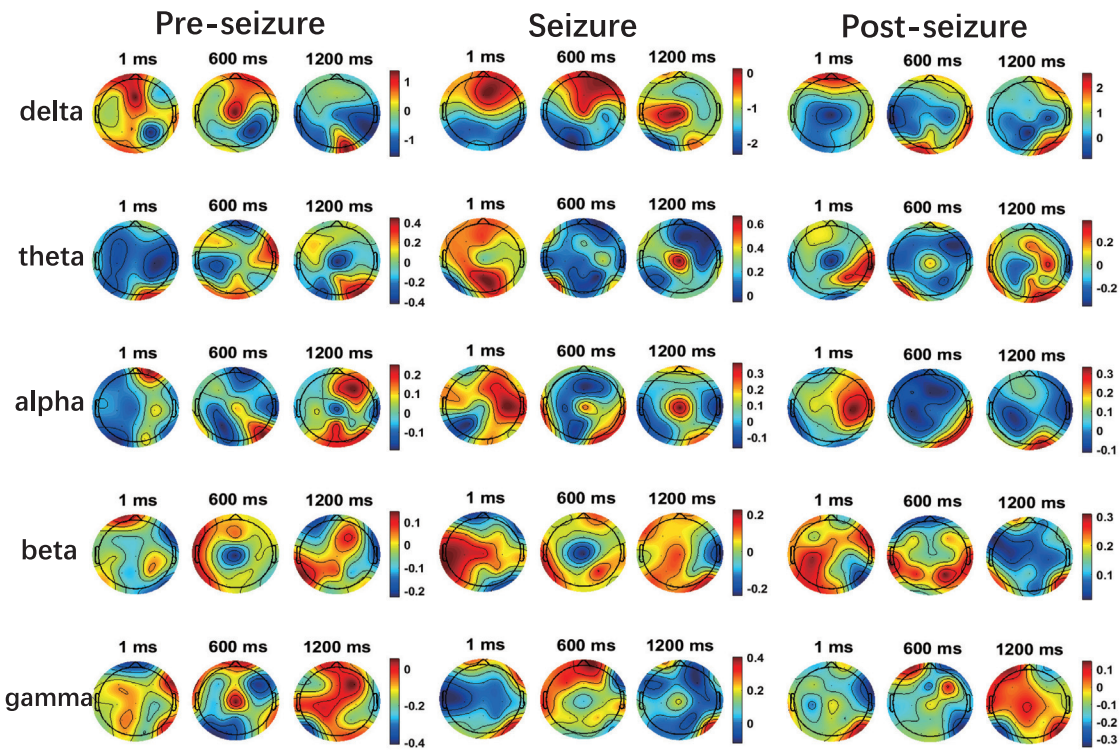


**Fig. 3.** The topographic maps of West syndrome in pre-seizure, seizure, and post-seizure of 5 sub-bands.

domain, frequency domain, and time-frequency domain are obtained for analysis in this paper. These different connection measurements, including correlation (Kendall et al., 1946), coherence (González, Rodriguez, Sagartzazu, Schumacher, & Isasa, 2010), TFCMI (Lu et al., 2011), PLV (Lachaux, Rodriguez, Martinerie, & Varela, 1999), PLI (Stam, Nolte, & Daffertshofer, 2007), and WPLI (Vinck, Oostenveld, Van Wingerden, Battaglia, & Pennartz, 2011), are calculated among different channels for functional connectivity study in this paper.<sup>1</sup>

### 3.2.1. Correlation

Correlation measures the linear dependence of two random variables. Particularly, the Pearson correlation on random variable with  $N$  observations is defined as

$$\rho(A, B) = \frac{1}{N-1} \sum_{i=1}^N \left( \frac{A_i - \mu_A}{\sigma_A} \right) \left( \frac{B_i - \mu_B}{\sigma_B} \right) \quad (3)$$

where  $\mu_A$  and  $\sigma_A$ ,  $\mu_B$  and  $\sigma_B$  are the mean and standard deviation of  $A$  and  $B$ , respectively. Therefore, the correlation coefficient between the two EEG signals can be calculated by (3). To help observe the correlation between channels, we visualized the average correlation matrix of 5 different frequency bands of the 3 states in the West syndrome. Fig. 4 shows pair-wised correlation among 19 EEG channels. The circle area and color both represent the absolute magnitude of the correlation matrix, indicating the strength of channel correlation. The larger the size of the circle is, the stronger the correlation will be. As observed, the similarity between 19 channels is high in the  $\delta$  band, but the number of these similar channels is gradually decreasing when the frequency band is increasing, as can be found from the gradually decreased similarity in non-adjacent electrodes to the Cz electrode.

<sup>1</sup> Other averaged correlation matrices are presented in supplementary documents due to page limitations (i.e. Coherence, TFCMI, PLV, PLI, WPLI).

### 3.2.2. Magnitude-squared coherence

Magnitude-squared coherence can evaluate the linear relationship between two signals in a specific frequency band or frequency point. Assume  $P_{xx}(f)$ ,  $P_{yy}(f)$ , and  $P_{xy}(f)$  are the power spectral density and the cross power spectral density at frequency  $f$ , the coherence of two EEGs is

$$C_{xy}(f) = \frac{|P_{xy}(f)|^2}{P_{xx}(f)P_{yy}(f)} \quad (4)$$

where the power spectral density is defined as  $P(f) = \frac{1}{N} \left| \sum_{n=0}^{N-1} x_n e^{-j2\pi f \Delta t n} \right|^2$ ,  $\frac{-1}{2\Delta t} < f \leq \frac{1}{2\Delta t}$ ,  $\Delta t$  is the sampling interval,  $P_{xy}(\omega) = \sum_{m=-\infty}^{\infty} R_{xy}(m) e^{-j\omega m}$  is the cross power spectral density. Here,  $R_{xy}(m)$  is the cross-correlation as

$$R_{xy}(m) = E \{x_{n+m} y_n^*\} = E \{x_n y_{n-m}^*\} \quad (5)$$

where  $E\{\cdot\}$  is the expected value operator.

Apparently,  $C_{xy}(f)$  is within  $[0, 1]$ ,  $C_{xy}(f) = 0$  means the two variables are linear independence on the frequency  $f$ . The larger the coherence, the stronger the statistical dependence between the two signals. Although coherence is widely used in EEG connectivity analysis, it can only evaluate the linear dependence of two signals, and cannot detect the non-linear relationship between them. The indicator is also easily affected by signal amplitude. A high correlation between Fp1, Fp2, F3, F4, F7, F8, T3, T4, T5, and T6 channels can be observed. It indicates that there has a synchronization of brain activity in the frontal and temporal regions. Meanwhile, the correlation between these channels gradually decreases along with the increase of frequency.

### 3.2.3. Time frequency cross mutual information

TFCMI uses the mutual information to calculate the time-frequency nonlinear relationship of two signals, thereby assessing the similarity. The cross-channel Morlet is applied for time-spectrum (power) calculation with the frequency resolution

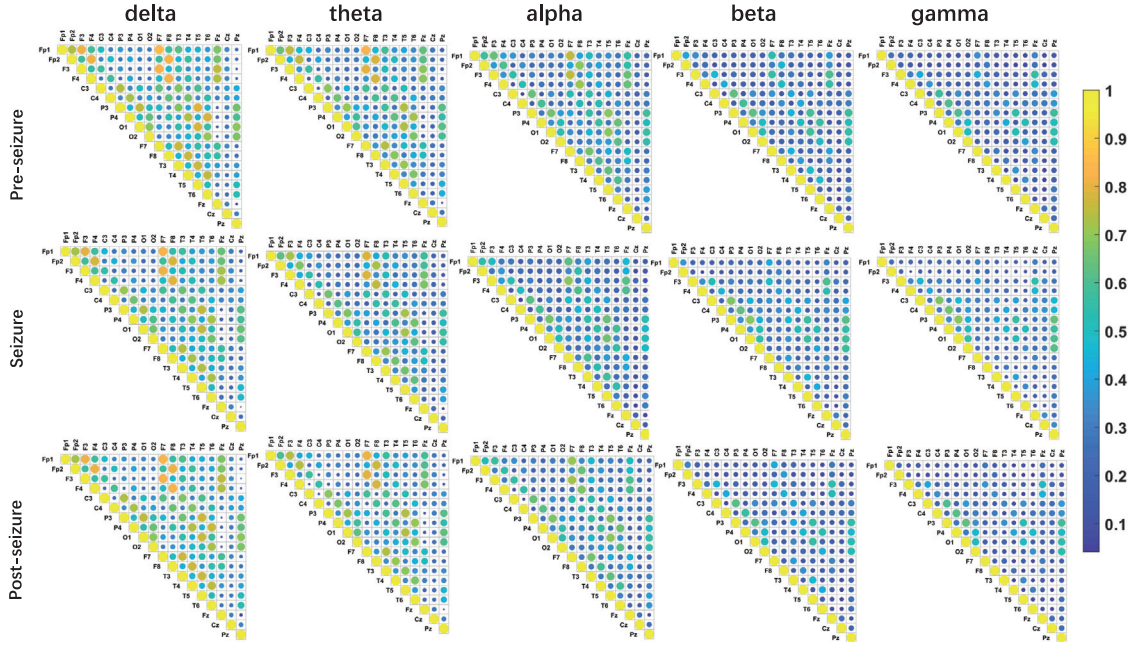


**Fig. 4.** Average correlation matrices in different sub-bands of West syndrome.

of 0.1 Hz in this paper. The definition of Morlet wavelet transform is

$$W_{xi}(t, f) = \int x_i(\lambda) \cdot \overline{\phi_{t,f}(t-\lambda)} d\lambda \quad (6)$$

where  $x_i(t)$  is EEG of  $i$ th channel, the Morlet wavelet is  $\phi_{t,f}(\lambda) = A \cdot e^{i2\pi f(\lambda-t)} e^{-\frac{-(\lambda-1)^2}{2\sigma^2}}$  with time spread of  $\sigma = \frac{8}{2\pi f}$ ,  $A = (\sigma\sqrt{2})^{-1/2}$  and  $\overline{\phi_{t,f}(\lambda)}$  is the complex conjugates of  $\phi_{t,f}(\lambda)$ . and their time spread is defined by  $\sigma = \frac{8}{2\pi f}$ . The normalization factor is  $A = (\sigma\sqrt{2})^{-1/2}$  and  $\overline{\phi_{t,f}(\lambda)}$  are the complex conjugates of  $\phi_{t,f}(\lambda)$ . Denote the averaged power of the  $i$ th channel by a random variable  $F_i$  and the probability density function (PDF) by  $p(F_{i,b})$ , the entropy of  $F_i$  is obtained by  $H(F_i) = -\sum_{b=1}^{50} p(F_{i,b}) \ln p(F_{i,b})$ . The joint entropy  $H(F_i, F_j)$  between the  $i$ th and  $j$ th channel EEGs can be estimated using the joint PDF  $p(F_{i,b}, F_{j,b})$  as  $H(F_i, F_j) = -\sum_{b=1}^{50} p(F_{i,b}, F_{j,b}) \ln p(F_{i,b}, F_{j,b})$

TFCMI of two random variables  $F_i$  and  $F_j$  is

$$\begin{aligned} \text{TFCMI}(F_i, F_j) &= H(F_i) + H(F_j) - H(F_i, F_j) \\ &= \sum_{b=1}^{50} p(F_{i,b}, F_{j,b}) \ln \frac{p(F_{i,b}, F_{j,b})}{p(F_{i,b}) p(F_{j,b})} \end{aligned} \quad (7)$$

TFCMI is a robust index measuring the functional connectivity based on the average power variation of EEG. The value of TFCMI ranges from 0 to 1. A larger value means a higher coupling strength between the two EEGs. Particularly, a strong coupling between frontotemporal regions can be observed, and the coupling gradually decreases along with the increase of frequency bands.

#### 3.2.4. Phase-Locking Value

PLV is an important indicator for the synchronization of biological signals. In EEG activity analysis, PLV is commonly used to measure task-induced remote synchronous changes in neural activity. Assume the phase difference sequence of two EEGs (2) is  $\Delta\varphi_n(t)$ , PLV is calculated by

$$\text{PLV} \triangleq \left| \frac{1}{N} \sum_{n=1}^N e^{j\Delta\varphi_n(t)} \right| \quad (8)$$

where  $N$  is the length of the phase difference sequence. PLV ranges from 0 to 1. PLV of 1 means that the phase difference sequence is a constant series and the phase difference is uniformly distributed in the range of  $[0, 2\pi]$ . A similar trend to the coherence can be found in PLV.

#### 3.2.5. Phase Lag Index

PLI measures the non-zero phase difference synchronization between two signals. Unlike PLV, PLI discards phase synchronization for phase differences that take the remainder of  $\pi$  as zero. PLI is less susceptible to volumetric conduction effects and active reference electrodes. PLI is defined as

$$\text{PLI} \triangleq \left| \frac{1}{N} \sum_{n=1}^N \text{sign}(\Delta\varphi_n(t)) \right| \quad (9)$$

Similarly, PLI ranges from 0 to 1. A large PLI means that more asymmetry exists in the phase difference distribution and higher possibility of the existence of real connectivity presents between two EEGs. As observed, via PLI, poor synchronization between brain regions can be found. Even though, the variability of the matrices in 3 different states is significant. This may be caused by the interference in PLI by the co-source problem.

#### 3.2.6. Weighted Phase Lag Index

In general, using scalp EEG in seizure detection does not completely avoid homologous interference. To address the insensitive to common source problems in PLI, WPLI is derived for further evaluation. Assume  $Z$  is the cross-spectrum of two EEGs, WPLI is defined as

$$\text{WPLI} \equiv \frac{|E\{\Im(Z)\}|}{E\{\Re(Z)\}} = \frac{|E\{|\Im(Z)| \text{ sign}(\Im(Z))\}|}{E\{|(\Im(Z))\|_2\}} \quad (10)$$

where  $\Im(Z)$  is the imaginary part of  $Z$ . WPLI weights the cross spectrum by the imaginary part, meaning WPLI is insensitive to additional uncorrelated noises and therefore enables a better assessment of the connectivity between EEGs. WPLI ranges from 0 to 1. A larger WPLI indicates a higher coupling of nerve oscillatory activity. The average WPLI correlation matrix of West syndrome in different brain rhythm waves reveals that (1) the coupling between all channels gradually decreases along with the frequency

band increases, (2) the correlation matrices of the 3 states are significantly different in  $\delta$ ,  $\alpha$  and  $\beta$  bands.

Overall, the correlation, coherence, TFCMI, PLV, PLI, and WPLI of 5 sub-bands in pre-seizure, seizure, and post-seizure states of West syndrome are derived, where these connection values between all nodes are integrated to an adjacency matrix to generate a weighted network. Different to conventional binary network, which dichotomizes the weights between nodes by thresholding, the proposed adjacency matrix based weighted network is more feasible in characterizing the degree of coherence and connectivity between brain regions. Moreover, a one-tailed paired t-test is performed to assess the significant changes of the coherence between the 3 different stages of brain regions in West syndrome.

### 3.3. Correlation analysis

Graph theory provides a quantitative analysis for complex brain networks. The commonly utilized network parameters can be broadly classified into local parameters (node degree, clustering coefficient, local efficiency, etc.) and global parameters (feature path length, global efficiency, etc.) (Agosta et al., 2013). To investigate the local and global properties of the functional network before and after West's seizure, the following network indicators are analyzed in this study.

#### 3.3.1. Clustering coefficient ( $C$ )

Measures the clustering tendency of nodes in the graph (Clemente & Grassi, 2018), which can be derived by

$$C = \frac{1}{N} \sum_{i=1}^N \frac{\sum_{j,k} A_{ij} A_{jk} A_{ki}}{\sum_i k_i (k_i - 1)} \quad (11)$$

where  $N$  is the number of network nodes,  $A$  is the adjacency matrix,  $k_i = \sum_j A_{ij}$ ,  $C$  is the average of local clustering coefficients of all vertices. A large  $C$  indicates the high connection density of nodes in the network.

#### 3.3.2. Feature path length ( $PL$ )

Assesses the connectivity level of nodes in the network (Newman, 2003), defined as

$$L = \frac{1}{N(N-1)} \sum_{i \in N} \sum_{j \in N, i \neq j} d_{ij} \quad (12)$$

where  $d_{i,j}$  is the shortest path length between nodes  $i$  and  $j$ . The smaller the value, the more efficient the information transfer between two nodes and the better the connectivity of the network will be.

#### 3.3.3. Global efficiency ( $Ge$ )

Measures the efficiency of remote information transmission in a network (Guimera & Amaral, 2005). It is the inverse of the average characteristic PL between all nodes in the network, defined as

$$E_{global} = \frac{1}{N(N-1)} \sum_{j,k \in G_i} \frac{1}{L_{j,k}} \quad (13)$$

where  $L_{j,k}$  is the average feature path between nodes  $i$  and  $j$ .  $Ge$  represents the average effect of the relevant brain network and can represent the overall information transmission capacity of the brain's network.

#### 3.3.4. Local efficiency ( $Le$ )

Measures the average efficiency of information transfer within a local subgraph or neighborhood (Latora & Marchiori, 2001), defined as

$$E_{local} = \frac{1}{N_{G_i} (N_{G_i} - 1)} \sum_{j,k \in G_i} \frac{1}{L_{j,k}} \quad (14)$$

where  $N_{G_i}$  is the number of nodes of subnetwork  $G_i$ . The higher the local efficiency, the more efficient the information is transmitted within the local network, and the less differentiated the network is.

The clustering coefficient and local efficiency express the functional connectivity effects between brain regions and reflect the ability of brain networks to process local information, while the global efficiency and feature path length reflect the ability of the brain network to process global information. The above network topology parameters are calculated via the Brain Connectivity toolbox (Rubinov & Sporns, 2010). The  $19 \times 19$  connection matrix for each band is taking as input to calculate  $C$ ,  $PL$ ,  $Ge$ ,  $Le$ . These parameters are first detected as conforming to a normal distribution. Subsequently, a multi-factor analysis of variance (ANOVA) is applied to analyze the variability of the parameters in the 3 different states, where the significance level threshold is adjusted to 0.05. Fig. 5 shows the network topology parameter distributions for all samples in pre-seizure, seizure, and post-seizure states of West syndrome based on coherence. Detailed discussion to the network topology parameters will be given in the subsequent section.<sup>2</sup>

Algorithm 1 summarizes the analysis method of West Syndrome functional networks.

---

#### Algorithm 1: West Syndrome Analysis Algorithm

---

##### 1 Input:

2 EEG database  $N = \{N_i\}$ , Input  $X \in \mathbb{R}^{D \times H \times W}$ , Number of categories  $K = 3$ .

##### 3 Output:

4 functional connectivity patterns, Network topology metrics

##### 5 Processing stage:

1. while  $k \leq K$  do

(a) Extraction of brain rhythms

(b) Calculate the correlation matrix(correlation, coherence, TFCMI, PLI, WPLI, PLV)

(c)  $k \leftarrow k + 1$

2. end while

3. Perform one-tailed paired t-test:  $t = \frac{\bar{x} - \mu}{s/\sqrt{n}}$

4. Obtain brain functional connectivity patterns

5. Calculate network topology parameters ( $C$ ,  $Ge$ ,  $Le$ ,  $PL$ )

6. Perform multi-factor ANOVA

---

## 4. Results and discussions

The study aims to determine whether the network feature differences could be applied for judging cluster spasm seizure prognosis and cessation prognosis, and the analysis is carried out using clinical EEGs from 15 patients diagnosed with West syndrome. Here, 19 electrodes are selected as brain network nodes. To clearly show the connectivity between brain regions, we used a two-tailed t-detection method to count the association matrix and find out the functional brain connectivity patterns.

<sup>2</sup> Other indexes based brain network parameter distributions are presented in the supplementary file (namely, Correlation, TFCMI, PLV, PLI, WPLI).

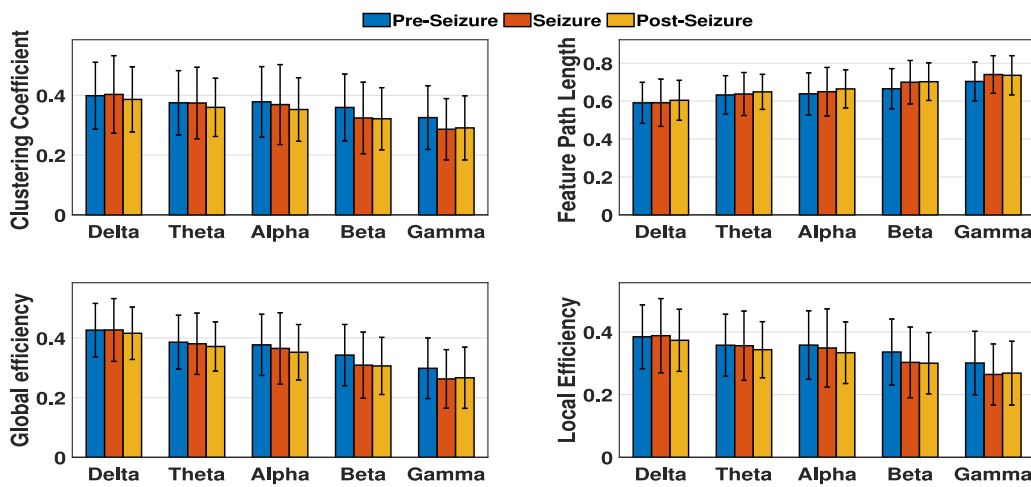


**Fig. 5.** The distributions of the coherence based network parameters, i.e., the mean  $C$ , PL, Ge, Le for all samples in pre-seizure, seizure, and post-seizure states of West syndrome, error lines represent the sample variance.

#### 4.1. Brain functional connectivity

Brain functional connectivity patterns can effectively show connectivity variability in specific bands. Fig. 6 shows the marginal differences in brain functional connectivity based on correlation, coherence, TFCMI, PLV, PLI, WPLI. Here, only the connectivity variation of 5 sub-bands in Pre-Seizure, Seizure, and Post-Seizure states of West syndrome for a particular brain network connectivity mode is compared.

**Correlation-based brain network connectivity analysis.** Comparing pre-seizure with seizure, significant differences including the increased or decreased connectivity in the  $\delta$ ,  $\theta$  and  $\alpha$  bands can be clearly found. However, for the  $\beta$  and  $\gamma$  bands, there is a tendency for all enhancement and the regional connectivity shows a weakening. For instance, the  $\beta$  band exhibits an attenuation of connectivity between the parietal and occipital regions. This may be related to the presence of muscle contraction and imbalance in postural-motor coordination during West seizure. In contrast, comparing seizure with post-seizure, it is found that the  $\beta$  and  $\gamma$  bands show significant variability in connectivity enhancement or reduction, while the other three bands show connectivity attenuation. But in the  $\delta$  band, the increased connectivity between right brain regions can be clearly observed. Similarly, in the  $\alpha$  band, an enhanced connection between the frontal pole and the lateral frontal area is presented. This may be caused by the significant changes in the patient's head movements during the West seizure. When comparing Pre-seizure and Post-seizure periods, a significant decrease in connectivity can be found in all sub-bands. When comparing with the coherence and correlation based brain network connectivity patterns, the connectivity differences are consistency in the two indicators, but only with subtle differences. Moreover, for  $\delta$ ,  $\theta$ , and  $\alpha$  sub-bands, all the connectivity patterns are enhanced in the right-brain scalp region during seizure when comparing with the post-seizure period.

**TFCMI-based brain network connectivity analysis.** A significant increase in connectivity can be found for the  $\alpha$ ,  $\beta$  and  $\gamma$  bands when comparing pre-seizures with respect to seizures. However, for the  $\delta$  and  $\theta$  bands, the inter-channel local connectivity is diminished, while the trend of enhancement increases. For example, in the  $\delta$  band, the connectivity shows a weakening in the region near the midline. Meanwhile, in the  $\theta$  band, the connectivity between the frontopolar and frontal regions is weakened. The connections between all regions of the 5 sub-bands are enhanced when comparing seizures with respect to post-seizures.

The comparisons between pre-seizures and post-seizures show that a significant increase in connectivity can be found in the  $\delta$ ,  $\theta$ , and  $\alpha$  bands, and a significant decrease in connectivity is also observed in the  $\beta$  and  $\gamma$  bands. Enhanced connectivity in the hindbrain region is presented in both  $\beta$  and  $\gamma$  bands.

The PLV-based brain network connectivity patterns analysis revealed essentially the similar characteristics to the correlation-based brain network connectivity property with subtle differences. Namely, when comparing seizures with respect to post-seizures, it also appears that the connectivity between right brain regions are enhanced in the  $\alpha$  band.

**PLI-based brain network connectivity patterns analysis.** Significant differences can be found in increased or decreased connectivity in the  $\beta$  and  $\gamma$  bands when comparing pre-seizures with respect to seizures. In the  $\delta$  band, the connectivity is reduced in all brain regions. In the  $\theta$  band, there is no significant change in connectivity. In contrast, in the  $\alpha$  band, the brain connectivity is reduced in the left brain region. Comparing seizures with post-seizures, the connectivity is significantly weakened in all sub-bands. In contrast, in the  $\gamma$  band, the connectivity in a small number of regions are enhanced. When comparing pre-Seizure with post-Seizure, the connectivity between temporal lobe regions is significantly reduced in the  $\delta$  band, while the connectivity between anterior hemispheric regions is reduced in the  $\alpha$  band. For  $\beta$ ,  $\gamma$  bands, although the overall trend of diminished connectivity is evident, the local connectivity between the posterior half of the brain regions is enhanced.

**WPLI-based brain network connectivity patterns analysis.** When comparing pre-seizure with respect to seizure, there is a significant difference in diminished connectivity in the  $\delta$  band, enhanced connectivity in  $\theta$ ,  $\alpha$ , and  $\beta$  bands, and increased or decreased connectivity in the  $\gamma$  band. The same connectivity can be found when comparing seizure with respect to post-seizure. Moreover, when comparing pre-seizure with post-seizure, a clear enhanced connectivity in the  $\delta$ ,  $\theta$ , and  $\alpha$  bands can be observed. While for the  $\beta$  and  $\gamma$  bands, the opposite effect that the connectivity is reduced can be found.

Overall, for all brain network connectivity measurement metrics, the following conclusions are observed: (1) when comparing pre-seizures with respect to seizures, the connectivity of the parietal region, responsible for motor coordination, and the connectivity of occipital region, responsible for visual information processing, have shown opposite changes in the  $\beta$ ,  $\gamma$  band. (2) In contrast, in the bands of the main components of EEG in children, there is a significant difference between all brain regions with

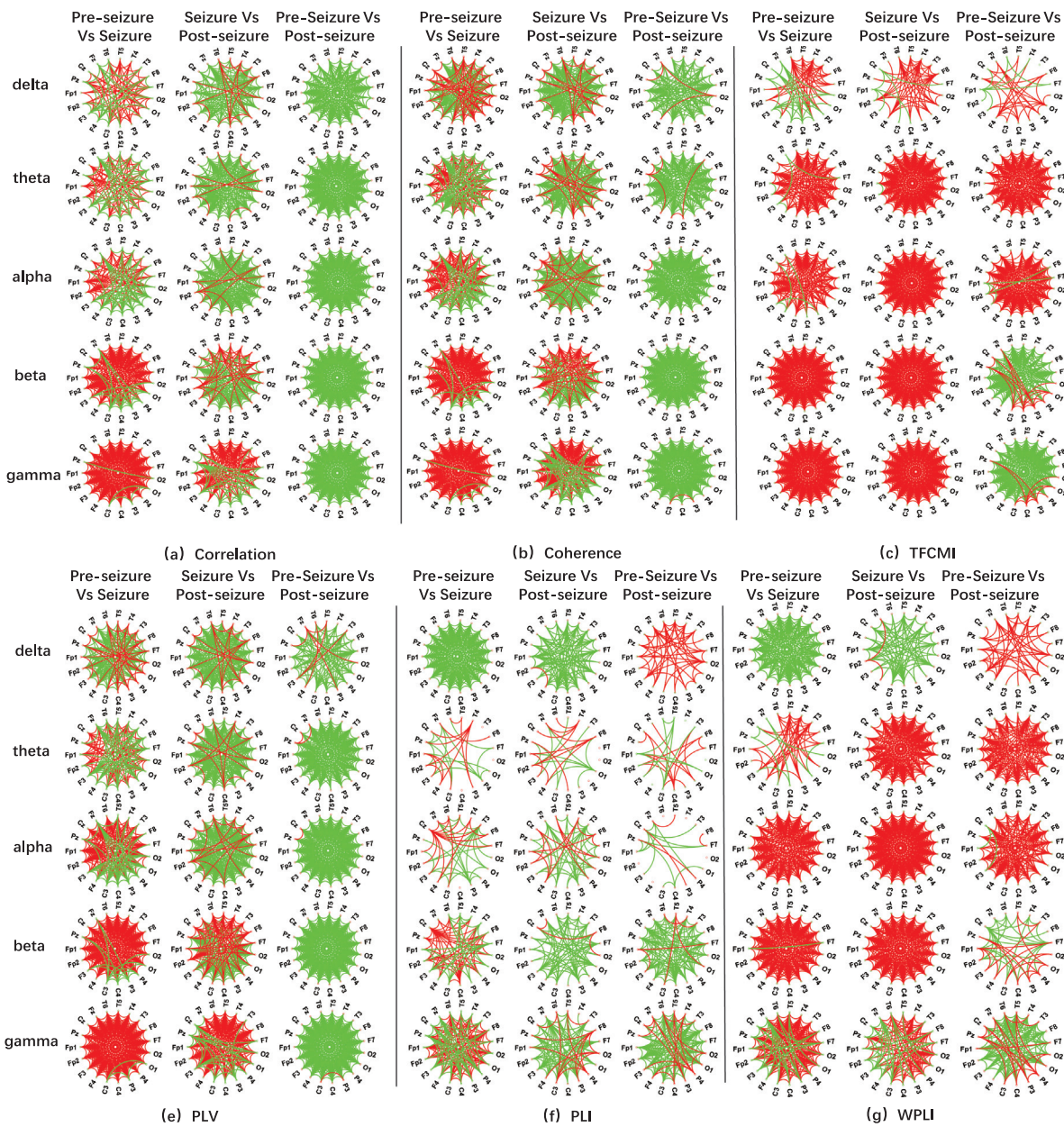


**Fig. 6.** Brain functional connectivity patterns in 5 sub-bands for 3 different states in West syndrome calculated based on 6 different association matrices, the inter-channel connectivity metric is counted by the two-tailed  $t$ -detection. In each subplot, red line represents the enhanced lead connectivity and the green line represents the diminished lead connectivity.

enhanced or reduced coherence. (3) When comparing seizure with respect to post-seizure, a significant asymmetry in the distribution of the intensity of left and right brain region connections in the  $\alpha$  band can be observed. (4) When comparing pre-seizure with post-seizure, it is found that the coherence between the frontopolar and temporal lobe regions is significantly diminished in the low frequency band. This can be interpreted as the damage to the cognitive and memory functions of the child with each series of spastic seizures.

#### 4.2. Network topology metrics

All the network topology metric parameters for the 5 sub-bands in Fig. 5 show that all the parameters calculated for the 6 different weighted networks present the same trend of change. Along with gradually growth of the frequency bands, 4 network topology parameters ( $C$ ,  $PL$ ,  $Ge$ ,  $Le$ ) gradually decrease, and the

trend of the feature path length reverses. In other words, as the frequency band increases, the brain's ability to process global and local information becomes weaker. It is also understood that the  $\delta$  and  $\theta$  bands are the main bands for building global and local connectivity in the brain network regardless of the situation.

For each of the 5 sub-bands with different network connectivity patterns, the variability of the network topology metrics for pre-seizure, seizure, and post-seizure are derived for comparisons, where the detailed results are shown in Table 2. As observed, the values of  $C$ ,  $Ge$ , and  $Le$  in the 3 different states continue to decrease while the  $PL$  values increase in the  $\theta$ ,  $\alpha$ , and  $\beta$  bands. *It reflects that brain networks continue to become less efficient in processing global and local information during the seizure cycle.* In the  $\delta$  band, the ability of the brain network to process local information is first enhanced and then diminished during the seizure cycle, while the efficiency of global information processing is decreasing. In the  $\gamma$  band, the ability of the

**Table 2**

Statistical results of network parameters of 6 brain network connection mode.

	Band	C			PL			Ge			Le			P			
		Pre-seizure	Seizure	Post-seizure	P												
Correlation	delta	0.494±0.128	0.492±0.136	0.475±0.115	***	0.425±0.112	0.435±0.122	0.441±0.106	***	0.541±0.093	0.538±0.102	0.528±0.086	***	0.482±0.113	0.485±0.123	0.465±0.103	***
	theta	0.452±0.128	0.451±0.141	0.428±0.114	***	0.497±0.115	0.509±0.128	0.519±0.105	***	0.499±0.095	0.494±0.108	0.481±0.086	***	0.441±0.115	0.439±0.127	0.421±0.102	***
	alpha	0.451±0.144	0.443±0.158	0.406±0.131	***	0.527±0.128	0.546±0.144	0.571±0.118	***	0.484±0.111	0.471±0.125	0.449±0.101	***	0.437±0.113	0.428±0.143	0.396±0.118	***
	beta	0.419±0.148	0.368±0.162	0.351±0.142	***	0.581±0.134	0.634±0.147	0.646±0.128	***	0.44±0.118	0.395±0.13	0.385±0.113	***	0.403±0.135	0.356±0.147	0.341±0.129	***
	gamma	0.395±0.162	0.309±0.161	0.218±0.172	***	0.616±0.148	0.692±0.154	0.685±0.156	***	0.405±0.135	0.344±0.138	0.346±0.145	***	0.377±0.149	0.3±0.154	0.307±0.159	***
	delta	0.399±0.112	0.403±0.13	0.386±0.109	***	0.591±0.108	0.591±0.125	0.604±0.105	***	0.426±0.09	0.427±0.105	0.416±0.088	***	0.384±0.102	0.388±0.118	0.373±0.099	***
Coherence	theta	0.375±0.108	0.374±0.12	0.36±0.098	***	0.633±0.102	0.637±0.114	0.649±0.092	***	0.386±0.09	0.381±0.103	0.372±0.083	***	0.358±0.099	0.356±0.111	0.343±0.089	***
	alpha	0.378±0.118	0.369±0.134	0.353±0.106	***	0.638±0.111	0.649±0.128	0.664±0.101	***	0.377±0.103	0.365±0.112	0.352±0.098	***	0.358±0.106	0.349±0.125	0.334±0.099	***
	beta	0.359±0.112	0.324±0.12	0.322±0.104	***	0.665±0.106	0.7±0.115	0.702±0.099	***	0.343±0.103	0.309±0.111	0.306±0.096	***	0.336±0.105	0.303±0.113	0.309±0.098	***
	gamma	0.325±0.107	0.286±0.103	0.291±0.107	***	0.704±0.102	0.74±0.099	0.736±0.104	***	0.298±0.102	0.263±0.098	0.267±0.103	***	0.301±0.101	0.264±0.097	0.268±0.102	***
	delta	0.587±0.042	0.586±0.045	0.588±0.043	***	0.411±0.04	0.412±0.044	0.41±0.042	***	0.589±0.041	0.588±0.044	0.589±0.042	***	0.587±0.04	0.586±0.045	0.586±0.043	***
	theta	0.5±0.043	0.496±0.043	0.505±0.046	***	0.499±0.043	0.503±0.043	0.492±0.046	***	0.501±0.043	0.497±0.043	0.507±0.046	***	0.5±0.043	0.496±0.043	0.505±0.046	***
TFCMI	alpha	0.422±0.043	0.418±0.042	0.428±0.045	***	0.576±0.043	0.58±0.042	0.571±0.045	***	0.424±0.043	0.42±0.042	0.429±0.045	***	0.422±0.043	0.418±0.042	0.428±0.045	***
	beta	0.548±0.056	0.319±0.051	0.343±0.051	***	0.65±0.056	0.679±0.051	0.655±0.056	***	0.35±0.056	0.321±0.051	0.345±0.056	***	0.348±0.056	0.319±0.051	0.343±0.056	***
	gamma	0.248±0.063	0.214±0.055	0.238±0.056	***	0.749±0.064	0.783±0.053	0.762±0.057	***	0.251±0.064	0.217±0.055	0.238±0.057	***	0.248±0.063	0.214±0.055	0.235±0.056	***
	delta	0.549±0.1	0.557±0.107	0.54±0.094	***	0.437±0.096	0.432±0.102	0.446±0.091	**	0.548±0.082	0.554±0.089	0.541±0.077	***	0.523±0.091	0.53±0.099	0.514±0.086	***
	theta	0.481±0.096	0.482±0.109	0.462±0.084	***	0.524±0.098	0.529±0.103	0.541±0.088	***	0.484±0.078	0.481±0.091	0.467±0.07	***	0.458±0.087	0.457±0.1	0.44±0.077	***
	alpha	0.458±0.104	0.446±0.124	0.421±0.099	***	0.56±0.099	0.574±0.116	0.595±0.102	***	0.454±0.086	0.441±0.106	0.423±0.082	***	0.434±0.095	0.423±0.114	0.401±0.091	***
PLV	beta	0.396±0.1	0.35±0.117	0.348±0.107	***	0.625±0.091	0.669±0.108	0.671±0.097	***	0.39±0.084	0.35±0.099	0.349±0.089	***	0.374±0.094	0.332±0.108	0.33±0.098	***
	gamma	0.365±0.133	0.291±0.133	0.305±0.144	***	0.657±0.123	0.724±0.123	0.711±0.134	***	0.356±0.116	0.297±0.114	0.309±0.126	***	0.344±0.124	0.277±0.123	0.289±0.134	***
	delta	0.272±0.064	0.287±0.068	0.278±0.066	***	0.594±0.115	0.558±0.122	0.583±0.117	***	0.4±0.072	0.422±0.074	0.408±0.073	***	0.304±0.066	0.321±0.07	0.311±0.068	***
	theta	0.21±0.041	0.21±0.047	0.21±0.039	***	0.716±0.071	0.712±0.085	0.715±0.068	***	0.32±0.051	0.323±0.056	0.321±0.048	***	0.238±0.043	0.239±0.049	0.238±0.041	***
	alpha	0.159±0.031	0.159±0.043	0.157±0.026	***	0.801±0.041	0.797±0.076	0.803±0.034	***	0.247±0.04	0.248±0.056	0.246±0.034	***	0.181±0.033	0.182±0.047	0.18±0.028	***
	beta	0.102±0.025	0.01±0.021	0.098±0.014	***	0.874±0.029	0.874±0.028	0.878±0.016	***	0.16±0.032	0.161±0.03	0.156±0.02	***	0.117±0.027	0.116±0.023	0.113±0.016	***
WPLI	gamma	0.07±0.034	0.07±0.016	0.068±0.015	**	0.91±0.061	0.913±0.023	0.914±0.027	**	0.113±0.05	0.114±0.031	0.112±0.032	**	0.081±0.038	0.081±0.019	0.079±0.018	**
	delta	0.465±0.099	0.309±0.081	0.474±0.098	***	0.221±0.122	0.528±0.145	0.207±0.115	***	0.606±0.084	0.441±0.084	0.614±0.082	***	0.502±0.095	0.443±0.082	0.51±0.094	***
	theta	0.397±0.086	0.384±0.081	0.414±0.091	***	0.344±0.134	0.349±0.135	0.317±0.131	***	0.537±0.079	0.534±0.082	0.554±0.081	***	0.434±0.084	0.43±0.089	0.45±0.088	***
	alpha	0.327±0.081	0.309±0.081	0.338±0.083	***	0.5±0.139	0.528±0.145	0.475±0.14	***	0.458±0.082	0.441±0.084	0.472±0.082	***	0.361±0.082	0.343±0.082	0.373±0.082	***
	beta	0.224±0.073	0.205±0.065	0.222±0.062	***	0.699±0.12	0.724±0.104	0.71±0.105	***	0.331±0.084	0.312±0.069	0.332±0.078	***	0.251±0.076	0.232±0.059	0.25±0.068	***
	gamma	0.144±0.06	0.137±0.035	0.14±0.041	**	0.813±0.102	0.82±0.068	0.819±0.075	**	0.225±0.078	0.222±0.055	0.223±0.06	**	0.164±0.065	0.157±0.039	0.161±0.045	**

• Data are the mean ± variance values of the parameters.

• Significance of differences between the 3 status of West syndrome (ANOVA, \*: p&lt;0.05, \*\*: p&lt;0.01, \*\*\*: p&lt;0.001).

• C: Clustering coefficient; PL: feature path length; Ge: Global efficiency; Le: Local efficiency.

brain network to process local and global information is first diminished and then enhanced.

The results on coherence reveal that the efficiency of brain networks in processing local and global information is first enhanced and then weakened in  $\delta$  and  $\gamma$  bands, but the efficiency is consistently weakened in  $\alpha$  and  $\beta$  bands. For PLV, similar observations can be found to the coherence based analysis. Based on for TFCMI and WPLI, all frequency bands exhibit the phenomenon that brain network processing efficiency of local and global information first diminishes and then enhances during the seizure cycle. While for PLI, the variability of network topological parameters is not significant. In the  $\delta$  and  $\gamma$  bands, the brain networks show dispersion in their ability to process information during the seizure cycle. This may be related to the synchronization of brain area activity that occurs during West seizures. This is because the PLI index is more limited for solving the co-source problem.

The analysis is carried out by combining the weighted network principle with the statistical results of the parameters. Based on the results of signal amplitude, frequency, and phase (i.e., correlation, coherence, and PLV), it is found that the trend of variation of variability in  $\theta$ ,  $\alpha$ , and  $\beta$  bands is consistent. In contrast, in the  $\delta$  and  $\gamma$  bands, the opposite trend changes significantly during a seizure cycle. In other words, there is a sudden change in the ability to process global and local information during west seizure. However, the brain's ability to process post-seizure is very different from pre-seizure. Based on mutual information (e.g., TFCMI, WPLI), all frequency bands show a weakened ability to process global and local information during seizures and return to normal after the seizure ends.

In summary, combining the statistical results of brain functional connectivity patterns and brain network topological parameters, more pronounced changes in brain regions and the topological parameters of brain network maps with large changes in opposite trends can be used as biomarkers for predicting seizure onset and end of cascade spasm seizures. For instance, the connectivity patterns and network parameter changes in the  $\delta$  band can be adopted to determine West seizure cessation

prognosis. Similarly, the corresponding changes in the  $\gamma$  band can be used for West seizure prediction.

## 5. Conclusions

In this paper, the scalp EEG based functional connectivity and network topology parameters have been analyzed for the prognosis of childhood West's seizure cycle. The medical statistics and anatomical principles have been combined to explore the brain mechanisms of West's seizures, which are very valuable for clinical research implications. The study is carried out on the EEG data of 15 children suffered from West syndrome, and the analysis reveals that (1) there exists asymmetry property in connectivity between left and right brain regions during the seizure cycle, (2) significant changes in the strength of connectivity occurred between parietal and occipital regions, and between frontopolar and temporal lobe regions, (3) the corresponding local and global efficiencies of brain networks present stage-specific differences. To further investigate the mechanism of West's seizure cycle, future research will focus on (1) combining functional magnetic resonance imaging (fMRI) and EEG signals to assess the effects of West seizures on functional connectivity patterns in the brain, (2) developing machine learning based West seizure cycle prediction model with the brain functional connectivity patterns, (3) analyzing individual subject differences and performing a comprehensive analysis by adding normal control groups.

## Ethical standards

This study has been approved by the Children's Hospital, Zhejiang University School of Medicine and registered in Chinese Clinical Trial Registry (ChiCTR1900028804). All patients gave their informed consent prior to their inclusion in the study.

## Declaration of competing interest

The authors declare that they have no known competing financial interests or personal relationships that could have appeared to influence the work reported in this paper.

## Appendix A. Supplementary data

Supplementary material related to this article can be found online at <https://doi.org/10.1016/j.neunet.2022.05.029>.

## References

- Abela, E., Pawley, A. D., Tangwiriyasakul, C., Yaakub, S. N., Chowdhury, F. A., Elwes, R. D., et al. (2019). Slower alpha rhythm associates with poorer seizure control in epilepsy. *Annals of Clinical and Translational Neurology*, 6(2), 333–343.
- Agosta, F., Sala, S., Valsasina, P., Meani, A., Canu, E., Magnani, G., et al. (2013). Brain network connectivity assessed using graph theory in frontotemporal dementia. *Neurology*, 81(2), 134–143.
- Baker, S. N. (2007). Oscillatory interactions between sensorimotor cortex and the periphery. *Current Opinion in Neurobiology*, 17(6), 649–655.
- Bernardo, D., Nariai, H., Hussain, S. A., Sankar, R., & Wu, J. Y. (2020). Interictal scalp fast ripple occurrence and high frequency oscillation slow wave coupling in epileptic spasms. *Clinical Neurophysiology*, 131(7), 1433–1443.
- Bernhardt, B. C., Bonilha, L., & Gross, D. W. (2015). Network analysis for a network disorder: the emerging role of graph theory in the study of epilepsy. *Epilepsy & Behavior*, 50, 162–170.
- Cao, J., Chen, L., Hu, D., Dong, F., Jiang, T., Gao, W., et al. (2021). Unsupervised eye blink artifact detection from EEG with Gaussian mixture model. *IEEE Journal of Biomedical and Health Informatics*, 25(8), 2895–2905. <http://dx.doi.org/10.1109/JBHI.2021.3057891>.
- Cao, J., Hu, D., Wang, Y., Wang, J., & Lei, B. (2021). Epileptic classification with deep transfer learning based feature fusion algorithm. *IEEE Transactions on Cognitive and Developmental Systems*.
- Cao, J., Zhu, J., Hu, W., & Kummert, A. (2020). Epileptic signal classification with deep EEG features by stacked CNNs. *IEEE Transactions on Cognitive and Developmental Systems*, 12(4), 709–722. <http://dx.doi.org/10.1109/TCDS.2019.2936441>.
- Capone, G., Goyal, P., Ares, W., & Lannigan, E. (2006). Neurobehavioral disorders in children, adolescents, and young adults with down syndrome. *American Journal of Medical Genetics Part C: Seminars in Medical Genetics*, 142(3), 158–172.
- Chu, Y.-J., Chang, C.-F., Weng, W.-C., Fan, P.-C., Shieh, J.-S., & Lee, W.-T. (2021). Electroencephalography complexity in infantile spasms and its association with treatment response. *Clinical Neurophysiology*, 132(2), 480–486.
- Clarke, A. R., Barry, R. J., McCarthy, R., & Selikowitz, M. (2001). EEG-defined subtypes of children with attention-deficit/hyperactivity disorder. *Clinical Neurophysiology*, 112(11), 2098–2105.
- Clemente, G. P., & Grassi, R. (2018). Directed clustering in weighted networks: A new perspective. *Chaos, Solitons & Fractals*, 107, 26–38.
- Cui, X., Cao, J., Hu, D., Wang, T., Jiang, T., & Gao, F. (2022). Regional scalp EEGs analysis and classification on typical childhood epilepsy syndromes. *IEEE Transactions on Cognitive and Developmental Systems*, 1. <http://dx.doi.org/10.1109/TCDS.2022.3175636>.
- Cui, X., Hu, D., Lin, P., Cao, J., Lai, X., Wang, T., et al. (2022). Deep feature fusion based childhood epilepsy syndrome classification from electroencephalogram. *Neural Networks*, 150, 313–325.
- Feng, Y., Zheng, R., Cui, X., Wang, T., Jiang, T., Gao, F., et al. (2022). 3D residual-attention-deep-network-based childhood epilepsy syndrome classification. *Knowledge-Based Systems*, 248, Article 108856.
- González, A. G., Rodriguez, J., Sagartzazu, X., Schumacher, A., & Isasa, I. (2010). Multiple coherence method in time domain for the analysis of the transmission paths of noise and vibrations with non stationary signals. In *Proceedings of ISMA 2010*.
- Guimera, R., & Amaral, L. A. N. (2005). Cartography of complex networks: modules and universal roles. *Journal of Statistical Mechanics: Theory and Experiment*, 2005(02), P02001.
- Guo, J., Li, H., Sun, X., Qi, L., Qiao, H., Pan, Y., et al. (2021). Detecting high frequency oscillations for stereoelectroencephalography in epilepsy via hypergraph learning. *IEEE Transactions on Neural Systems and Rehabilitation Engineering*, 29, 587–596. <http://dx.doi.org/10.1109/TNSRE.2021.3056685>.
- Hu, D., Cao, J., Lai, X., Liu, J., Wang, S., & Ding, Y. (2020). Epileptic signal classification based on synthetic minority oversampling and blending algorithm. *IEEE Transactions on Cognitive and Developmental Systems*, 13(2), 368–382.
- Hu, D., Cao, J., Lai, X., Wang, Y., Wang, S., & Ding, Y. (2020). Epileptic state classification by fusing hand-crafted and deep learning EEG features. *IEEE Transactions on Circuits and Systems II: Express Briefs*, 68(4), 1542–1546.
- Hu, D. K., Mower, A., Shrey, D. W., & Lopour, B. A. (2020). Effect of interictal epileptiform discharges on EEG-based functional connectivity networks. *Clinical Neurophysiology*, 131(5), 1087–1098.
- Hughes, J. R. (2008). Gamma, fast, and ultrafast waves of the brain: their relationships with epilepsy and behavior. *Epilepsy & Behavior*, 13(1), 25–31.
- Hussein, R., Lee, S., Ward, R., & McKeown, M. J. (2021). Semi-dilated convolutional neural networks for epileptic seizure prediction. *Neural Networks*, 139, 212–222. <http://dx.doi.org/10.1016/j.neunet.2021.03.008>. URL <https://www.sciencedirect.com/science/article/pii/S0893608021000885>.
- Janicot, R., Shao, L.-R., & Stafstrom, C. E. (2020). Infantile spasms: an update on pre-clinical models and EEG mechanisms. *Children*, 7(1), 5.
- Kendall, M. G., et al. (1946). The advanced theory of statistics. *The Advanced Theory of Statistics*, (2nd Ed).
- Lachaux, J.-P., Rodriguez, E., Martinerie, J., & Varela, F. J. (1999). Measuring phase synchrony in brain signals. *Human Brain Mapping*, 8(4), 194–208.
- Latora, V., & Marchiori, M. (2001). Efficient behavior of small-world networks. *Physical Review Letters*, 87(19), Article 198701.
- Li, C., Sohrabpour, A., Jiang, H., & He, B. (2021). High-frequency hubs of the ictal cross-frequency coupling network predict surgical outcome in epilepsy patients. *IEEE Transactions on Neural Systems and Rehabilitation Engineering*, 29, 1290–1299. <http://dx.doi.org/10.1109/TNSRE.2021.3093703>.
- Lin, Y., Du, P., Sun, H., Liang, Y., Wang, Z., Cui, Y., et al. (2021). Identifying refractory epilepsy without structural abnormalities by fusing the common spatial patterns of functional and effective EEG networks. *IEEE Transactions on Neural Systems and Rehabilitation Engineering*, 29, 708–717. <http://dx.doi.org/10.1109/TNSRE.2021.3071785>.
- Lu, C.-F., Teng, S., Hung, C.-L., Tseng, P.-J., Lin, L.-T., Lee, P.-L., et al. (2011). Reorganization of functional connectivity during the motor task using EEG time-frequency cross mutual information analysis. *Clinical Neurophysiology*, 122(8), 1569–1579.
- McCrimmon, C. M., Riba, A., Garner, C., Maser, A. L., Phillips, D. J., Steenari, M., et al. (2021). Automated detection of ripple oscillations in long-term scalp EEG from patients with infantile spasms. *Journal of Neural Engineering*, 18(1), Article 016018.
- Milikovsky, D. Z., Weissberg, I., Kamintsky, L., Lippmann, K., Schefenbauer, O., Frigerio, F., et al. (2017). Electrocorticographic dynamics as a novel biomarker in five models of epileptogenesis. *Journal of Neuroscience*, 37(17), 4450–4461.
- Miltner, W. H., Braun, C., Arnold, M., Witte, H., & Taub, E. (1999). Coherence of gamma-band EEG activity as a basis for associative learning. *Nature*, 397(6718), 434–436.
- Newman, M. E. (2003). The structure and function of complex networks. *SIAM Review*, 45(2), 167–256.
- Oppenheim, A. V. (1999). *Discrete-time signal processing*. Pearson Education India.
- Pavone, P., Polizzi, A., Marino, S. D., Corsello, G., Falsaperla, R., Marino, S., et al. (2020). West syndrome: a comprehensive review. *Neurological Sciences*, 1–16.
- Pavone, P., Striano, P., Falsaperla, R., Pavone, L., & Ruggieri, M. (2014). Infantile spasms syndrome, west syndrome and related phenotypes: what we know in 2013. *Brain and Development*, 36(9), 739–751.
- Raghav, S., Sriram, N., Temel, Y., Rao, S. V., & Kubben, P. L. (2020). EEG based multi-class seizure type classification using convolutional neural network and transfer learning. *Neural Networks*, 124, 202–212. <http://dx.doi.org/10.1016/j.neunet.2020.01.017>. URL <https://www.sciencedirect.com/science/article/pii/S0893608020300198>.
- Rosch, R., Baldeweg, T., Moeller, F., & Baier, G. (2018). Network dynamics in the healthy and epileptic developing brain. *Network Neuroscience*, 2(1), 41–59.
- Rubinov, M., & Sporns, O. (2010). Complex network measures of brain connectivity: uses and interpretations. *Neuroimage*, 52(3), 1059–1069.
- Shrey, D. W., McManus, O. K., Rajaraman, R., Ombao, H., Hussain, S. A., & Lopour, B. A. (2018). Strength and stability of EEG functional connectivity predict treatment response in infants with epileptic spasms. *Clinical Neurophysiology*, 129(10), 2137–2148.
- Stacey, W., Kramer, M., Gunnarsdottir, K., Gonzalez-Martinez, J., Zaghloul, K., Inati, S., et al. (2020). Emerging roles of network analysis for epilepsy. *Epilepsy Research*, 159, Article 106255.
- Stam, C. J., Nolte, G., & Daffertshofer, A. (2007). Phase lag index: assessment of functional connectivity from multi channel EEG and MEG with diminished bias from common sources. *Human Brain Mapping*, 28(11), 1178–1193.
- Vinck, M., Oostenveld, R., Van Wingerden, M., Battaglia, F., & Pennartz, C. M. (2011). An improved index of phase-synchronization for electrophysiological data in the presence of volume-conduction, noise and sample-size bias. *Neuroimage*, 55(4), 1548–1565.
- Wang, J., Cao, J., Hu, D., Jiang, T., & Gao, F. (2021). Eye blink artifact detection with novel optimized multi-dimensional electroencephalogram features. *IEEE Transactions on Neural Systems and Rehabilitation Engineering*, 29, 1494–1503. <http://dx.doi.org/10.1109/TNSRE.2021.3099232>.
- Wen, D., Li, R., Jiang, M., Li, J., Liu, Y., Dong, X., et al. (2021). Multi-dimensional conditional mutual information with application on the EEG signal analysis for spatial cognitive ability evaluation. *Neural Networks*, <http://dx.doi.org/10.1016/j.neunet.2021.12.010>. URL <https://www.sciencedirect.com/science/article/pii/S0893608021004834>.
- Xu, Z., Wang, T., Cao, J., Bao, Z., Jiang, T., & Gao, F. (2021). BECT spike detection based on novel EEG sequence features and LSTM algorithms. *IEEE Transactions on Neural Systems and Rehabilitation Engineering*, 29, 1734–1743. <http://dx.doi.org/10.1109/TNSRE.2021.3107142>.